

Theory of magnetoroton bands in moiré materials

Bishoy M. Kousa,^{1,*} Nicolás Morales-Durán,^{1,2,*} Tobias M. R. Wolf,¹ Eslam Khalaf,³ and Allan H. MacDonald¹

¹Department of Physics, The University of Texas at Austin, Austin, Texas 78712, USA

²Center for Computational Quantum Physics, Flatiron Institute, New York, New York 10010, USA

³Department of Physics, Harvard University, Cambridge, Massachusetts 02138, USA

(Dated: February 26, 2025)

The recent realizations of the Hofstadter butterfly and fractional Chern insulators in moiré materials have introduced a new ingredient, a periodic lattice potential, to the study of quantum Hall phases. While the fractionalized states in moiré systems are expected to be in the same universality class as their counterparts in Landau levels, the periodic potential can have qualitative and quantitative effects on physical observables. Here, we examine how the magnetoroton collective modes of fractional quantum Hall (FQH) states are altered by external periodic potentials. Employing a single-mode-approximation, we derive an effective Hamiltonian for the low-energy neutral excitations expressed in terms of three-point density correlation functions, which are computed using Monte Carlo. Our analysis is applicable to FQH states in graphene with a hexagonal boron nitride (hBN) substrate and also to fractional Chern insulator (FCI) states in twisted MoTe₂ bilayers. We predict experimentally testable trends in the THz absorption characteristics of FCI and FQH states and estimate the external potential strength at which a soft-mode phase transition occurs between FQH and charge density wave (CDW) states.

Introduction — The interplay between strong magnetic fields and periodic potentials in the quantum physics of two-dimensional electrons has been a subject of enduring interest since Hofstadter’s 1976 discovery [1] of the butterfly pattern of gaps in the energy spectrum of a square-lattice tight-binding model. The Hofstadter butterfly was until recently mostly a theoretical curiosity [2–5] because of the impossibility of applying magnetic fields on the scale of flux quanta per the surface unit cell area to natural crystals. Recently, however, the longer periods of moiré materials [6–9] have made direct studies of excitation gaps at relevant magnetic field scales a reality, and in doing so have made it clear [10, 11] that interactions, which produce additional magnetic-field-dependent gaps, often play a major role. In this context, the recent observation of FCI states [12–17] in tMoTe₂ [18–21] and in rhombohedral graphene aligned with hexagonal boron nitride [22] has added an exciting new element to studies of the interplay between topological order [23] and lattice translational symmetry. Fractionalized ground states in moiré systems are in the same universality class as the Laughlin state [24], so one would expect their long-wavelength, low-energy neutral excitations to be similar to the magnetorotons of FQH systems [25, 26]. However, the presence of discrete translation symmetry should modify the collective excitations and enrich their behavior, giving rise to noticeable differences that lead to experimentally observable consequences.

In this Letter we investigate the simplest example of the interplay between periodic potentials, interaction-induced excitation gaps, band topology and strong magnetic fields by examining how the neutral excitations of the gapped Laughlin FQH state evolve when a periodic potential is added to the Hamiltonian. The external potential mixes the magnetoroton [25, 26] excitations and folds their dispersion into the Brillouin zone defined by the periodicity. We find that magnetoroton mixing is governed by the equal-time three-point density correlation function of the Laughlin state, which we evaluate using Monte Carlo simulations. As the periodic potential is made stronger,

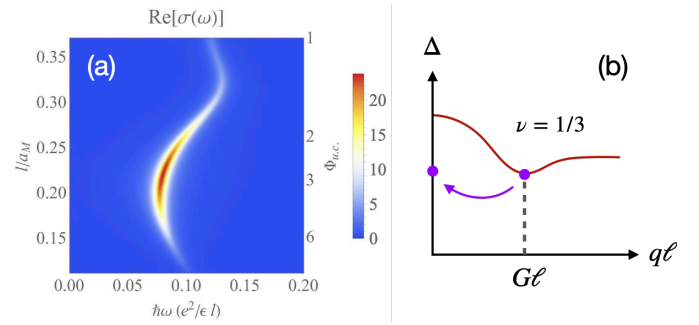


FIG. 1. (a) Magnetoroton band THz absorption as a function of the ratio of the magnetic length to the moiré period, in units of $\lambda^2(e^2/4\hbar)\nu$ where λ is the periodic potential strength and ν is the Landau Level filling factor [cf. Eq. (7)]. A system of interest can be adjusted to the strong absorption regime either by varying the magnetic field or by varying the moiré period. In tMoTe₂ fractional quantum anomalous Hall states the THz absorption is weak but can be strengthened by applying an external magnetic field. The absorption is maximized when the number of flux quanta per unit cell $\Phi_{u.c.} \approx 2.82$, which is realized at magnetic field $B \approx 15\text{T}$ for a 30 nm moiré. (b) Schematic illustration of the THz conductivity mechanism. The periodic potential mixes magnetoroton states at reciprocal lattice vectors \mathbf{G} into the ground state and transitions to magnetoroton states at the same \mathbf{G} are consequently dipole active.

the minimum of the lowest magnetoroton band decreases, suggesting a soft-mode instability of the Laughlin state toward a competing Wigner crystal state that has an integer (with Chern number $C = 0$ or 1) rather than a fractional quantum Hall effect. The periodic potential also mixes moiré reciprocal lattice vector magnetoroton excitations into the ground state, and as recognized previously [27], by doing so makes the THz range intra-Landau-level excitations infrared active. Here we show that the coupling with THz radiation is strongly enhanced when the periodic potential’s primitive reciprocal lattice vectors align with the undisturbed systems’ magnetoroton dispersion minimum, as illustrated in Fig. 1.

Our theory applies most naturally to fractional quantum Hall states in the $N = 0$ Landau level of graphene [28, 29] with a moiré pattern induced either by alignment to hBN [30] or by a twist between hBN layers [31–33] in the substrate. It also applies to the fractional Chern insulators in tMoTe₂ [18–21], since its layer-pseudospin Berry phases can be represented [34, 35] by an effective magnetic field with one flux quantum per moiré unit cell [36]. Our work emphasizes the intimate relationship between FCI and FQH states and explains the wide range of twist angles over which FCI states are observed in tMoTe₂.

Magnetoroton bands — We consider the Landau levels generated by a constant magnetic field, B_0 , in the presence of a weak periodic potential $V(\mathbf{r})$. The cyclotron gap is given by $\hbar\omega_c = eB_0/m$, where e and m are the electron's charge and mass, respectively. We assume that the cyclotron gap is the largest energy scale in the problem, so that the low-energy physics is well approximated by projecting to the lowest Landau level (LLL). When electronic interactions are added, the many-body Hamiltonian for the LLL in the presence of the periodic potential is

$$H = H_0 + V(\mathbf{r}) = \frac{1}{2A} \sum_{\mathbf{q}} V_{\mathbf{q}} \bar{\rho}_{\mathbf{q}} \bar{\rho}_{-\mathbf{q}} + \sum_{\mathbf{G}} \lambda_{\mathbf{G}} \bar{\rho}_{\mathbf{G}}. \quad (1)$$

In Eq. (1), $V_{\mathbf{q}}$ is the Coulomb potential, A is the area of the system, and $\bar{\rho}_{\mathbf{q}}$ is the density operator projected to the LLL. The reciprocal lattice vectors of the periodic potential are denoted by \mathbf{G} and the coefficients $\lambda_{\mathbf{G}}$ determine the shape and strength of the potential. For concreteness, we will keep only the first shell of reciprocal lattice vectors since higher harmonics will be suppressed by the projection to the LLL, which involves a magnetic form factor $e^{-|\mathbf{G}|^2 \ell^2/4}$, where ℓ is the magnetic length. We consider specifically a C_6 -symmetric potential which is frequently relevant experimentally in graphene and transition metal dichalcogenide (TMD) platforms. Under these assumptions all six first-shell Fourier coefficients are real and equal, so we denote them simply by λ , which we take as a perturbative parameter.

We will focus on filling $\nu = 1/3$ of the LLL, which is the simplest FQH state, although our results also apply to $\nu = 2/3$ by applying a particle-hole transformation to Eq. (1). In such case, the ground state of Eq. (1) when $\lambda = 0$, which we denote $|\Psi_0\rangle$, is in the same universality class as the Laughlin state. When the periodic potential is turned-on perturbatively, we expect a similar state to still be a good approximation for the ground state. The periodic potential will mix different Landau levels, but this effect is sub-leading in the limit of very large $\hbar\omega_c$. Within the LLL the periodic potential couples states that differ by a reciprocal lattice vector, $|\Psi_{\mathbf{q}}\rangle$ and $|\Psi_{\mathbf{q}+\mathbf{G}}\rangle$. This will lead to a negative energy correction of order λ^2 for the Laughlin-like ground state, as is usual in second order perturbation theory, but $\sim \lambda$ for the excited states. We estimate the coefficient of the λ^2 correction for the ground state in the Supplemental Material (SM) [37] and show that it is sufficiently small such that this term can be neglected for the range of λ we consider.

The low-energy neutral excitations of Eq (1) in the absence of the potential, $\lambda = 0$, are well described by the single-mode approximation (SMA) [25, 26], *i.e.* states $|\Psi_{\mathbf{q}}\rangle$ with energy $\Delta_{\mathbf{q}}$ given by

$$|\Psi_{\mathbf{q}}\rangle = \frac{1}{\sqrt{N\bar{S}_{\mathbf{q}}}} \bar{\rho}_{\mathbf{q}} |\Psi_0\rangle, \quad \Delta_{\mathbf{q}} = \frac{\bar{f}_{\mathbf{q}}}{\bar{S}_{\mathbf{q}}}, \quad (2)$$

where N is the number of electrons and the *projected oscillator strength* is defined as

$$\bar{f}_{\mathbf{q}} = \frac{1}{2N} \langle [\bar{\rho}_{\mathbf{q}}^\dagger, [H_0, \bar{\rho}_{\mathbf{q}}]] \rangle_0, \quad (3)$$

and the *projected structure factor* is

$$\bar{S}_{\mathbf{q}} = \frac{1}{N} \langle \bar{\rho}_{\mathbf{q}}^\dagger \bar{\rho}_{\mathbf{q}} \rangle_0 = S_{\mathbf{q}} - \left(1 - e^{-q^2 \ell^2/2}\right). \quad (4)$$

In Eq. (4) $S_{\mathbf{q}}$ is the full structure factor, and $\langle \dots \rangle_0 \equiv \langle \Psi_0 | \dots | \Psi_0 \rangle$. The magnetoroton gap in the SMA, Eq. (2), can be computed using that the projected density operators satisfy the GMP algebra $[\bar{\rho}_{\mathbf{q}}, \bar{\rho}_{\mathbf{k}}] = (\exp(q^* k \ell^2/2) - \exp(k^* q \ell^2/2)) \bar{\rho}_{\mathbf{q}+\mathbf{k}}$, where $q = q_x + i q_y$ [38].

We would like to determine how introducing $\lambda \neq 0$ affects the magnetoroton modes. As commented above, the periodic potential mixes SMA states related by a reciprocal lattice vector, but does not mix states within the Brillouin zone. We therefore expand the Hamiltonian (including the periodic potential) in terms of the SMA states, Eq. (2):

$$(h_{\mathbf{q}})_{\mathbf{G}, \mathbf{G}'} = \Delta_{\mathbf{q}+\mathbf{G}} \delta_{\mathbf{G}, \mathbf{G}'} + \lambda \frac{\langle \bar{\rho}_{\mathbf{q}+\mathbf{G}}^\dagger \bar{\rho}_{\mathbf{G}-\mathbf{G}'} \bar{\rho}_{\mathbf{q}+\mathbf{G}'} \rangle_0}{N \sqrt{\bar{S}_{\mathbf{k}+\mathbf{G}} \bar{S}_{\mathbf{k}+\mathbf{G}'}}}, \quad (5)$$

where \mathbf{q} is now restricted to the Brillouin zone of the periodic potential, $\mathbf{G} - \mathbf{G}'$ belongs to the first-shell of reciprocal lattice vectors and $\Delta_{\mathbf{q}}$ is the magnetoroton dispersion given by Eq. (2) see the SM [37] for a derivation of this expression [39]. The magnetoroton bands are obtained by diagonalizing $h_{\mathbf{q}}$ for all \mathbf{q} in the Brillouin zone.

The off-diagonal terms in Eq. (5) involve the three-point correlation function of the Laughlin state projected to the LLL. The latter is related to the unprojected three-point function:

$$\begin{aligned} \langle \bar{\rho}_{\mathbf{q}_1}^\dagger \bar{\rho}_{\mathbf{q}'} \bar{\rho}_{\mathbf{q}_2} \rangle_0 &= \langle \bar{\rho}_{\mathbf{q}_1}^\dagger \rho_{\mathbf{q}'} \rho_{\mathbf{q}_2} \rangle_0 - F(\alpha_{\mathbf{q}'}^{q_1} + \alpha_{\mathbf{q}_2}^{q_1} + \alpha_{\mathbf{q}_2}^{-q'}) \\ &- \delta S_{\mathbf{q}_2} F(\alpha_{\mathbf{q}'}^{q_2}) - \delta S_{\mathbf{q}_1 - \mathbf{q}_2} F(\alpha_{\mathbf{q}_2}^{q_1}) - \delta S_{\mathbf{q}_1} F(\alpha_{\mathbf{q}_2}^{-q'}), \end{aligned} \quad (6)$$

where $\mathbf{q}' = \mathbf{q}_1 - \mathbf{q}_2$ due to momentum conservation, and we used short-hand notations $\delta S_{\mathbf{q}} = S_{\mathbf{q}} - 1$, $F(\alpha) = 1 - e^{-\alpha/2}$ and $\alpha_{\mathbf{q}_2}^{q_1} = q_1^* q_2 \ell^2$. Eq. (6) is a generalization of Eq. (4) to the three-body case (see the SM for its derivation [37]). In order to construct the Hamiltonian Eq. (5) we require values for the equal-time three-point correlation function with arbitrary momentum arguments, which we obtain from Monte Carlo sampling of Laughlin-state position distributions [40]. Using Eq. (6) we then compute the projected three-point function

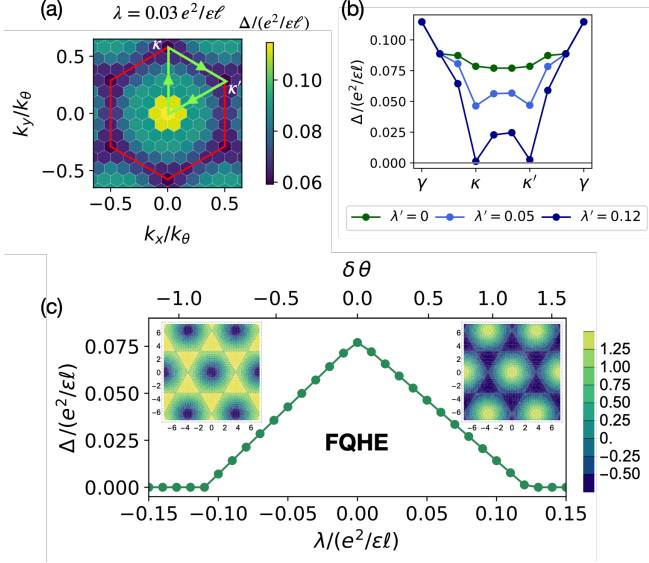


FIG. 2. (a) Lowest-energy magnetoroton band for $0 < \lambda < \lambda_c$, where λ_c is the critical value for the FCI–CDW transition. The magnitude of the first-shell reciprocal lattice vectors is k_θ . (b) Line-cut of the magnetoroton dispersion for several values of $\lambda' = \lambda/(e^2/\epsilon\ell)$ across a path in the Brillouin zone. The magnetoroton minima are at the κ/κ' points and become negative for $\lambda > \lambda_c^+$ or $\lambda < \lambda_c^-$, indicating an instability of the Laughlin-like state. (c) The magnetoroton gap Δ as a function of λ (bottom axis) and for the tMoTe₂ case the deviation $\delta\theta$ of the twist angle θ from the magic angle θ_m value (top axis). The insets indicate the symmetry of the periodic potential minima for positive and negative values of λ . We have truncated the reciprocal lattice to 25 vectors and sampled the Brillouin zone with 81 points. We have kept 2×10^5 MC samples.

which enters in the Hamiltonian Eq. (5). Eq. (6) and the Monte Carlo calculations are the two main technical elements of this work. Typical results for the magnetoroton bands are summarized in Fig. 2.

Soft-mode instability and competing Wigner crystal states — We focus first on the case of one flux quantum per unit cell of the periodic potential. The magnetoroton band evolution with potential strength λ in this case is relevant to the FCI states of tMoTe₂ at zero magnetic field. Close to the magic angle [41, 42], that we will denote θ_m , the continuum model for tMoTe₂ can be approximated by a LLL in a periodic potential [34, 35], therefore the effective value of λ is related to the deviation of the model parameters from magic angle values. Fig. 2(a) shows the lowest magnetoroton band for $\lambda/(e^2/\epsilon\ell) = 0.03$ and Fig. 2(b) displays line traces of the magnetoroton bands across the indicated path in the Brillouin zone, for several values of the potential strength. Results for higher magnetoroton bands are presented in the SM [37]. In the absence of the periodic potential the magnetoroton minimum is located near the centers of the edges of the Brillouin zone [43]. As λ is turned on, the minimum moves toward the κ/κ' Brillouin-zone corners. Soft modes at this wavevector would accompany a continuous phase transition to a $\sqrt{3} \times \sqrt{3}$ -unit-cell charge density wave. This

periodicity corresponds to three flux quanta and one electron per unit cell – the periodicity of the triangular-lattice Wigner crystal state that is expected to compete with the FCI state. The soft mode condensation should be taken as an indication of instability towards Wigner crystals, but ultimately we expect the transition to be first-order not continuous. We see that the value of the magnetoroton minimum decreases as λ is increased – eventually reaching zero at λ_c . Figure 2(c) shows the value of the magnetoroton gap as a function of λ and also as a function of the deviation $\delta\theta$ from the magic angle $\theta_m \approx 3.0^\circ$. We have taken continuum model parameters from [44] and $\epsilon = 20$ to convert between λ and θ .

We note that if we had added perturbative corrections up to order λ^2 in Eq. (5) there would be a small increase in the values of λ_c , but this would only represent a higher order quantitative correction to the phase diagram presented in Fig. 2(c). The potential strength at which the transition to a CDW occurs is larger for $\lambda > 0$ (a honeycomb potential – corresponding to a hole Wigner crystal) than for $\lambda < 0$ (an electron Wigner crystal), in correspondence with the relative stability of the electron Wigner crystal. Fig. 2(c) indicates that in MoTe₂ the $\nu = 2/3$ FCI state will be more stable than the $\nu = 1/3$ FCI state for twist angles smaller than the magic angle. Our calculations also explain the large twist angle ranges over which the FCI state has been observed.

THz conductivity – A simple expression for the THz intra-band conductivity $\text{Re } \sigma(\omega)$ based on a perturbative treatment of the external potential and single-mode-approximations similar to those employed here was derived previously in Ref. [27]:

$$\text{Re } \sigma(\omega) \approx \frac{e^2}{4\hbar} \nu \sum_{\mathbf{G}} \ell^2 |\mathbf{G}|^2 \frac{|\lambda_{\mathbf{G}}|^2}{\Delta_{\mathbf{G}}} \bar{S}_{\mathbf{G}} \delta(\hbar\omega - \Delta_{\mathbf{G}}), \quad (7)$$

where \mathbf{G} is a first-shell reciprocal lattice vector, $\nu = n_e/n_{\text{LL}}$ is the LL filling fraction for electron density $n_e = N/A$ and $n_{\text{LL}} = 1/(2\pi\ell^2)$. This expression for $\text{Re } \sigma(\omega)$ can be derived by taking the long wavelength limit of the corresponding approximate dynamic structure factor expression,

$$S(\mathbf{q}, \epsilon) \approx \sum_{\mathbf{G}} \left| \frac{\lambda_{\mathbf{G}} \langle \bar{\rho}_{\mathbf{q}+\mathbf{G}} \bar{\rho}_{\mathbf{q}} \bar{\rho}_{\mathbf{G}} \rangle_0}{N \Delta_{\mathbf{G}} \sqrt{\bar{S}_{\mathbf{q}+\mathbf{G}}}} \right|^2 \delta(\epsilon - \Delta_{\mathbf{q}+\mathbf{G}}), \quad (8)$$

and observing that since there are no dipole allowed transitions within the lowest Landau level, then $\bar{\rho}_{\mathbf{q}} |\Psi_0\rangle = 0$ to first order in $|\mathbf{q}|$, so the three-point function can be approximated as

$$\frac{\langle \bar{\rho}_{\mathbf{q}+\mathbf{G}} \bar{\rho}_{\mathbf{q}} \bar{\rho}_{\mathbf{G}} \rangle_0}{N \bar{S}_{\mathbf{q}+\mathbf{G}}} \approx i\ell^2 (\mathbf{q} \times \mathbf{G}) \cdot \hat{z}. \quad (9)$$

Eq. (7) was used to construct Fig. 1, see the SM [37] for details on its derivation. In Fig. 3 (a) we compare line traces for typical $\sigma(\omega)$ results obtained from Eq. (9) with those computed using Monte Carlo. In the SM [37], we compare Eq. (9) with numerical correlation functions for different \mathbf{q} and Monte Carlo sample sizes. The excellent agreement provides

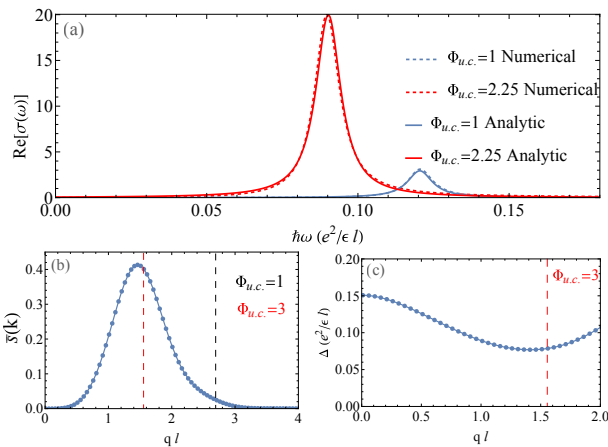


FIG. 3. (a) Comparison of optical conductivity calculated using Eq. (7) [solid lines] and Monte Carlo three-point correlation functions in Eq. (8) [dashed lines] for different number of flux quanta piercing each unit cell $\Phi_{u.c.}$. (b) Projected structure factor for the Laughlin state ($\nu = 1/3$) using the MC fitted coefficients [25]. The black dashed line indicates the magnitude of the moiré reciprocal lattice vector \mathbf{G} in the tMoTe₂ relevant case of one flux quantum per unit cell. The red dashed line indicates $|\mathbf{G}|$ for 3 flux quanta per unit cell, near the structure factor maximum (roton minimum). (c) Magnetoroton dispersion for the Laughlin state at $\nu = 1/3$. The projected structure factor maximum corresponds to the roton minimum, suggesting a competing charge density wave state.

assurance that the magnetoroton band calculations are accurate. Monte Carlo three-point correlation functions are the building blocks of our theory, they are related to non-linear response properties [45, 46] of quantum Hall systems and may find further applications [47].

Some of us [40] have previously argued that the magnetorotons of tMoTe₂ FCI states are optically dark. To see that this conclusion is consistent with Eq. (7), we note that for one flux quantum per unit cell $|\mathbf{G}|\ell = 2(\pi/\sqrt{3})^{1/2} \approx 2.7$. At this large wavevector $\bar{S}_{\mathbf{G}} \approx 0$ [see Fig. 3 (b)], implying that the optical conductivity remains small even for a relatively strong effective external potential. However, one can see from Eq. (7) that if the period of the external potential or the magnetic field strength is tuned so that it coincides approximately with the peak in the structure factor (and the magnetoroton minimum [c.f. Fig. 3 (b-c)]), magnetorotons become accessible to THz spectroscopy. This behavior was illustrated in Fig. 1 [48]. For tMoTe₂ the direction of the effective magnetic field and the applied external magnetic field are always the same. It follows that the magnetic field strength needed to bring the magnetoroton minima and the moiré reciprocal lattice vector must supply ≈ 1.7 flux quantum per cell - requiring magnetic fields ~ 100 T for typical MoTe₂ moiré periods. We therefore conclude that the THz oscillator strength of magnetoroton modes will remain small in laboratory magnetic fields. For the $N = 0$ Landau levels of graphene aligned to hBN, the effective periodic potential is strongest at alignment which yields a moiré period $a_M \sim 14$ nm. In this case THz coupling

to magnetoroton modes is maximized at $B \sim 68$ T - still an inconveniently strong magnetic field. We conclude that the optimal strategy to enable THz studies of magnetorotons is to form a long-period thBN moiré in the dielectric stack [31–33]. For example a 30 nm moiré period brings the magnetic field strength at which the maximum absorption happens down to $B \sim 15$ T.

Discussion — Even though they are not optically accessible in the absence of external perturbation, the low-energy excitations of FQH have been observed experimentally using inelastic light scattering [49–54] techniques. Away from the long-wavelength chiral graviton limit [55], the mechanism for the light scattering signal is poorly understood but thought to be disorder activated and to give a signal proportional to the magneto-roton density of states. Here we have shown that the presence of a periodic potential makes the magnetoroton modes optically active. At laboratory scale magnetic fields, we have shown that the optimal period for an external potential that is intended to make magnetoroton modes visible in THz spectroscopy is ~ 30 nm. Periodic potentials with periods in this range have been realized using thBN [33], but could also be realized by periodic patterning of gate dielectrics [56, 57] or by other nanolithography techniques. We believe that recent progress with van der Waals heterojunction devices finally brings THz optical probes of FQH and FCI collective modes within reach.

The single-mode approximation we employ is accurate when only one collective mode at each wavevector couples strongly to external potentials. The SMA is accurate for Laughlin states at wavevectors up to intermediate values [25, 26], but fails at large wavevectors where the lowest energy excitations are fractional particle-hole excitations that have very small oscillator strengths. In that limit the SMA energy may be viewed as an oscillator-strength weighted average over a continuum of excitations. This average energy should still accurately capture the small influence the lowest magneto-roton band due to mixing with large reciprocal lattice vectors basis states. The failure of the SMA to describe fractional quasiparticle-quasihole excitations should therefore not limit its ability to describe the lowest magneto-roton band.

The framework that we have developed here to describe the collective modes of FCI and periodically modulated FQH states, which is based on the SMA and on the calculation of three-point equal time correlation functions, is complementary to more direct numerical approaches developed by other authors [27, 40, 58–64]. As developed here it applies only to $\nu = 1/m$ Laughlin states. Generalizations to other FQH states, for instance those in the Jain sequence [65, 66], could be attempted based on composite fermion exciton [67, 68] picture of their collective excitations. Our conclusion that patterning on the 30 nm length scale will enable THz probes of FQH state collective modes, applies equally well to all FQH states, many of which have rich incompletely-understood collective excitation spectra.

Acknowledgments – The Flatiron Institute is a division of the Simons Foundation. We acknowledge HPC resources provided by the Texas Advanced Computing Center at The University

of Texas at Austin. This work was supported by a Simons Foundation Collaborative Research Grant, by Robert A. Welch Foundation Grant F-2112, in part by grant NSF PHY-2309135 to the Kavli Institute for Theoretical Physics (KITP) and in part by NSF MRSEC DMR-2308817 through the Center for Dynamics and Control of Materials. B.M.K. acknowledges the hospitality of the Flatiron Institute where part of this work has been performed.

* These authors contributed equally to this work

- [1] D. R. Hofstadter, Energy levels and wave functions of bloch electrons in rational and irrational magnetic fields, *Phys. Rev. B* **14**, 2239 (1976).
- [2] F. H. Claro and G. H. Wannier, Magnetic subband structure of electrons in hexagonal lattices, *Phys. Rev. B* **19**, 6068 (1979).
- [3] F. Claro, Spectrum of tight binding electrons in a square lattice with magnetic field, *physica status solidi (b)* **104**, K31 (1981).
- [4] A. H. MacDonald, Landau-level subband structure of electrons on a square lattice, *Phys. Rev. B* **28**, 6713 (1983).
- [5] A. H. MacDonald, Quantized hall effect in a hexagonal periodic potential, *Phys. Rev. B* **29**, 3057 (1984).
- [6] C. R. Dean, L. Wang, P. Maher, C. Forsythe, F. Ghahari, Y. Gao, J. Katoch, M. Ishigami, P. Moon, M. Koshino, T. Taniguchi, K. Watanabe, K. L. Shepard, J. Hone, and P. Kim, Hofstadter's butterfly and the fractal quantum hall effect in moiré superlattices, *Nature* **497**, 598 (2013).
- [7] L. A. Ponomarenko, R. V. Gorbachev, G. L. Yu, D. C. Elias, R. Jalil, A. A. Patel, A. Mishchenko, A. S. Mayorov, C. R. Woods, J. R. Wallbank, M. Mucha-Kruczynski, B. A. Piot, M. Potemski, I. V. Grigorieva, K. S. Novoselov, F. Guinea, V. I. Fal'ko, and A. K. Geim, Cloning of dirac fermions in graphene superlattices, *Nature* **497**, 594 (2013).
- [8] R. Bistritzer and A. H. MacDonald, Moiré butterflies in twisted bilayer graphene, *Phys. Rev. B* **84**, 035440 (2011).
- [9] E. Y. Andrei, D. K. Efetov, P. Jarillo-Herrero, A. H. MacDonald, K. F. Mak, T. Senthil, E. Tutuc, A. Yazdani, and A. F. Young, The marvels of moiré materials, *Nature Reviews Materials* **6**, 201 (2021).
- [10] Y. Xie, A. T. Pierce, J. M. Park, D. E. Parker, E. Khalaf, P. Ledwith, Y. Cao, S. H. Lee, S. Chen, P. R. Forrester, *et al.*, Fractional chern insulators in magic-angle twisted bilayer graphene, *Nature* **600**, 439 (2021).
- [11] C. R. Kometter, J. Yu, T. Devakul, A. P. Reddy, Y. Zhang, B. A. Foutty, K. Watanabe, T. Taniguchi, L. Fu, and B. E. Feldman, Hofstadter states and re-entrant charge order in a semiconductor moiré lattice, *Nature Physics* **19**, 1861 (2023).
- [12] H. Li, U. Kumar, K. Sun, and S.-Z. Lin, Spontaneous fractional chern insulators in transition metal dichalcogenide moiré superlattices, *Phys. Rev. Research* **3**, L032070 (2021).
- [13] T. Neupert, L. Santos, C. Chamon, and C. Mudry, Fractional quantum hall states at zero magnetic field, *Phys. Rev. Lett.* **106**, 236804 (2011).
- [14] K. Sun, Z. Gu, H. Katsura, and S. Das Sarma, Nearly flatbands with nontrivial topology, *Phys. Rev. Lett.* **106**, 236803 (2011).
- [15] D. N. Sheng, Z.-C. Gu, K. Sun, and L. Sheng, Fractional quantum hall effect in the absence of landau levels, *Nature Communications* **2**, 389 (2011).
- [16] N. Regnault and B. A. Bernevig, Fractional chern insulator, *Phys. Rev. X* **1**, 021014 (2011).
- [17] Y.-L. Wu, B. A. Bernevig, and N. Regnault, Zoology of fractional chern insulators, *Phys. Rev. B* **85**, 075116 (2012).
- [18] J. Cai, E. Anderson, C. Wang, X. Zhang, X. Liu, W. Holtzmann, Y. Zhang, F. Fan, T. Taniguchi, K. Watanabe, Y. Ran, T. Cao, L. Fu, D. Xiao, W. Yao, and X. Xu, Signatures of fractional quantum anomalous hall states in twisted mote2, *Nature* **622**, 63 (2023).
- [19] Y. Zeng, Z. Xia, K. Kang, J. Zhu, P. Knüppel, C. Vaswani, K. Watanabe, T. Taniguchi, K. F. Mak, and J. Shan, Thermodynamic evidence of fractional chern insulator in moiré mote2, *Nature* **622**, 69 (2023).
- [20] H. Park, J. Cai, E. Anderson, Y. Zhang, J. Zhu, X. Liu, C. Wang, W. Holtzmann, C. Hu, Z. Liu, T. Taniguchi, K. Watanabe, J.-H. Chu, T. Cao, L. Fu, W. Yao, C.-Z. Chang, D. Cobden, D. Xiao, and X. Xu, Observation of fractionally quantized anomalous hall effect, *Nature* **622**, 74 (2023).
- [21] F. Xu, Z. Sun, T. Jia, C. Xu, C. Li, Y. Gu, K. Watanabe, T. Taniguchi, B. Tong, J. Jia, Z. Shi, S. Jiang, Y. Zhang, X. Liu, and T. Li, Observation of integer and fractional quantum anomalous hall effects in twisted bilayer mote₂, *Phys. Rev. X* **13**, 031037 (2023).
- [22] Z. Lu, T. Han, Y. Yao, A. P. Reddy, J. Yang, J. Seo, K. Watanabe, T. Taniguchi, L. Fu, and L. Ju, Fractional quantum anomalous Hall effect in multilayer graphene, *Nature* **626**, 759 (2024).
- [23] X.-G. Wen, Topological orders and edge excitations in fractional quantum hall states, *Advances in Physics* **44**, 405 (1995).
- [24] R. B. Laughlin, Anomalous quantum hall effect: An incompressible quantum fluid with fractionally charged excitations, *Phys. Rev. Lett.* **50**, 1395 (1983).
- [25] S. M. Girvin, A. H. MacDonald, and P. M. Platzman, Magneto-roton theory of collective excitations in the fractional quantum hall effect, *Phys. Rev. B* **33**, 2481 (1986).
- [26] S. M. Girvin, A. H. MacDonald, and P. M. Platzman, Collective-excitation gap in the fractional quantum hall effect, *Phys. Rev. Lett.* **54**, 581 (1985).
- [27] F. Wu and A. H. MacDonald, Moiré assisted fractional quantum hall state spectroscopy, *Phys. Rev. B* **94**, 241108 (2016).
- [28] Y. Zhang, Y.-W. Tan, H. L. Stormer, and P. Kim, Experimental observation of the quantum hall effect and berry's phase in graphene, *Nature* **438**, 201 (2005).
- [29] K. S. Novoselov, Z. Jiang, Y. Zhang, S. V. Morozov, H. L. Stormer, U. Zeitler, J. C. Maan, G. S. Boebinger, P. Kim, and A. K. Geim, Room-temperature quantum hall effect in graphene, *Science* **315**, 1379 (2007), <https://www.science.org/doi/pdf/10.1126/science.1137201>.
- [30] E. M. Spanton, A. A. Zibrov, H. Zhou, T. Taniguchi, K. Watanabe, M. P. Zaletel, and A. F. Young, Observation of fractional chern insulators in a van der waals heterostructure, *Science* **360**, 62 (2018).
- [31] P. Zhao, C. Xiao, and W. Yao, Universal superlattice potential for 2d materials from twisted interface inside h-bn substrate, *npj 2D Materials and Applications* **5**, 38 (2021).
- [32] C. R. Woods, P. Ares, H. Nevison-Andrews, M. J. Holwill, R. Fabregas, F. Guinea, A. K. Geim, K. S. Novoselov, N. R. Walet, and L. Fumagalli, Charge-polarized interfacial superlattices in marginally twisted hexagonal boron nitride, *Nature Communications* **12**, 347 (2021).
- [33] D. S. Kim, R. C. Dominguez, R. Mayorga-Luna, D. Ye, J. Embley, T. Tan, Y. Ni, Z. Liu, M. Ford, F. Y. Gao, S. Arash, K. Watanabe, T. Taniguchi, S. Kim, C.-K. Shih, K. Lai, W. Yao, L. Yang, X. Li, and Y. Miyahara, Electrostatic moiré potential from twisted hexagonal boron nitride layers, *Nature Materials* **23**, 65 (2024).
- [34] J. Shi, N. Morales-Durán, E. Khalaf, and A. H. MacDonald, Adiabatic approximation and aharonov-casher bands in twisted

- homobilayer transition metal dichalcogenides, *Phys. Rev. B* **110**, 035130 (2024).
- [35] N. Morales-Durán, N. Wei, J. Shi, and A. H. MacDonald, Magic Angles and Fractional Chern Insulators in Twisted Homobilayer Transition Metal Dichalcogenides, *Phys. Rev. Lett.* **132**, 096602 (2024).
- [36] Fractional quantum Hall (FQH) states are sometimes referred to as fractional Chern insulator (FCI) states whenever a periodic external potential is present. In this manuscript we reserve the term FCI for states in which the quantum Hall effect survives to zero magnetic field.
- [37] See supplemental material for (a) Details on the Brillouin-zone-folded Hamiltonian and the expressions for the optical conductivity, (b) A derivation of the expression for the projected three-point correlation function, (c) A numerical examination of the long-wavelength limit of the three-point function entering optical conductivities, and (d) Line trace plots of higher magnetoroton bands.
- [38] The single-mode approximation is expected to be accurate for q small. For filling factor $\nu = 1/3$ the SMA accurately approximates the neutral gap for $|q|$ up to the magnetoroton minimum. For large $|q|$ the SMA energy is the oscillator-strength weighted average over a continuum of neutral excitations and the neutral excitations with the lowest energy are quasi-hole-quasi-electron bound pairs. The SMA still faithfully captures the influence of mixing between large and small $|q|$ on the lowest energy collective modes.
- [39] We note that the quasi-particle-quasi-hole excitations in the large q limit do not couple strongly to the magnetorotons, hence we do not consider them in our derivation.
- [40] T. M. R. Wolf, Y.-C. Chao, A. H. MacDonald, and J. J. Su, *Intraband collective excitations in fractional chern insulators are dark* (2024), [arXiv:2406.10709 \[cond-mat.str-el\]](https://arxiv.org/abs/2406.10709).
- [41] T. Devakul, V. Crépel, Y. Zhang, and L. Fu, Magic in twisted transition metal dichalcogenide bilayers, *Nature Communications* **12**, 6730 (2021).
- [42] N. Morales-Durán, J. Wang, G. R. Schleder, M. Angeli, Z. Zhu, E. Kaxiras, C. Repellin, and J. Cano, Pressure-enhanced fractional chern insulators along a magic line in moiré transition metal dichalcogenides, *Phys. Rev. Res.* **5**, L032022 (2023).
- [43] A. C. Balram and S. Pu, Positions of the magnetoroton minima in the fractional quantum hall effect, *The European Physical Journal B* **90**, 124 (2017).
- [44] C. Wang, X.-W. Zhang, X. Liu, Y. He, X. Xu, Y. Ran, T. Cao, and D. Xiao, Fractional chern insulator in twisted bilayer moiré, *Phys. Rev. Lett.* **132**, 036501 (2024).
- [45] R. L. Peterson, Formal theory of nonlinear response, *Reviews of Modern Physics* **39**, 69 (1967).
- [46] S. Gravel and N. Ashcroft, Nonlinear response theories and effective pair potentials, *Physical Review B—Condensed Matter and Materials Physics* **76**, 144103 (2007).
- [47] Q. Gao, R. A. Lanzetta, P. Ledwith, J. Wang, and E. Khalaf, *Bootstrapping the quantum hall problem* (2024), [arXiv:2409.10619 \[cond-mat.str-el\]](https://arxiv.org/abs/2409.10619).
- [48] In that figure we used a Lorentzian representation of the delta function $\delta(x) \approx \epsilon^2/\pi(x^2 + \epsilon^2)$, $\epsilon = 0.005$.
- [49] A. Pinczuk, B. S. Dennis, L. N. Pfeiffer, and K. West, Observation of collective excitations in the fractional quantum hall effect, *Phys. Rev. Lett.* **70**, 3983 (1993).
- [50] M. Kang, A. Pinczuk, B. S. Dennis, L. N. Pfeiffer, and K. W. West, Observation of multiple magnetorotons in the fractional quantum hall effect, *Phys. Rev. Lett.* **86**, 2637 (2001).
- [51] C. F. Hirjibehedin, I. Dujovne, A. Pinczuk, B. S. Dennis, L. N. Pfeiffer, and K. W. West, Splitting of long-wavelength modes of the fractional quantum hall liquid at $\nu = 1/3$, *Phys. Rev. Lett.* **95**, 066803 (2005).
- [52] J. G. Groschhaus, I. Dujovne, Y. Gallais, C. F. Hirjibehedin, A. Pinczuk, Y.-W. Tan, H. Stormer, B. S. Dennis, L. N. Pfeiffer, and K. W. West, Spin texture and magnetoroton excitations at $\nu = 1/3$, *Phys. Rev. Lett.* **100**, 046804 (2008).
- [53] I. V. Kukushkin, J. H. Smet, V. W. Scarola, V. Umansky, and K. von Klitzing, Dispersion of the excitations of fractional quantum hall states, *Science* **324**, 1044 (2009), <https://www.science.org/doi/pdf/10.1126/science.1171472>.
- [54] C. Hirjibehedin, I. Dujovne, I. Bar-Joseph, A. Pinczuk, B. Dennis, L. Pfeiffer, and K. West, Resonant enhancement of inelastic light scattering in the fractional quantum hall regime at $\nu = 1/3$, *Solid State Communications* **127**, 799 (2003), advances in Studies of Electrons in Low Dimensional Structures.
- [55] J. Liang, Z. Liu, Z. Yang, Y. Huang, U. Wurstbauer, C. R. Dean, K. W. West, L. N. Pfeiffer, L. Du, and A. Pinczuk, Evidence for chiral graviton modes in fractional quantum hall liquids, *Nature* **628**, 78 (2024).
- [56] C. Forsythe, X. Zhou, K. Watanabe, T. Taniguchi, A. Pasupathy, P. Moon, M. Koshino, P. Kim, and C. R. Dean, Band structure engineering of 2d materials using patterned dielectric superlattices, *Nature nanotechnology* **13**, 566 (2018).
- [57] J. Sun, S. A. Akbar Ghorashi, K. Watanabe, T. Taniguchi, F. Camino, J. Cano, and X. Du, Signature of correlated insulator in electric field controlled superlattice, *Nano Letters* **24**, 13600 (2024).
- [58] C. Repellin, T. Neupert, Z. Papić, and N. Regnault, Single-mode approximation for fractional chern insulators and the fractional quantum hall effect on the torus, *Phys. Rev. B* **90**, 045114 (2014).
- [59] H. Lu, H.-Q. Wu, B.-B. Chen, K. Sun, and Z. Y. Meng, *Interaction-driven roton condensation in $c = 2/3$ fractional quantum anomalous hall state* (2024), [arXiv:2403.03258 \[cond-mat.str-el\]](https://arxiv.org/abs/2403.03258).
- [60] H. Lu, B.-B. Chen, H.-Q. Wu, K. Sun, and Z. Y. Meng, Thermodynamic response and neutral excitations in integer and fractional quantum anomalous hall states emerging from correlated flat bands, *Phys. Rev. Lett.* **132**, 236502 (2024).
- [61] X. Shen, C. Wang, X. Hu, R. Guo, H. Yao, C. Wang, W. Duan, and Y. Xu, *Magnetorotons in moiré fractional chern insulators* (2024), [arXiv:2412.01211 \[cond-mat.str-el\]](https://arxiv.org/abs/2412.01211).
- [62] M. Long, H. Lu, H.-Q. Wu, and Z. Y. Meng, *Spectra of magnetoroton and chiral graviton modes of fractional chern insulator* (2025), [arXiv:2501.00247 \[cond-mat.str-el\]](https://arxiv.org/abs/2501.00247).
- [63] X. Hu, D. Xiao, and Y. Ran, Hyperdeterminants and composite fermion states in fractional chern insulators, *Phys. Rev. B* **109**, 245125 (2024).
- [64] J. F. Mendez-Valderrama, D. Mao, and D. Chowdhury, Low-energy optical sum rule in moiré graphene, *Phys. Rev. Lett.* **133**, 196501 (2024).
- [65] A. C. Balram, G. J. Sreejith, and J. K. Jain, Splitting of the girvin-macdonald-platzman density wave and the nature of chiral gravitons in the fractional quantum hall effect, *Phys. Rev. Lett.* **133**, 246605 (2024).
- [66] R. K. Dora and A. C. Balram, *Static structure factor and the dispersion of the girvin-macdonald-platzman density-mode for fractional quantum hall fluids on the haldane sphere* (2024), [arXiv:2410.00165 \[cond-mat.str-el\]](https://arxiv.org/abs/2410.00165).
- [67] R. K. Kamilla, X. G. Wu, and J. K. Jain, Excitons of composite fermions, *Phys. Rev. B* **54**, 4873 (1996).
- [68] R. K. Kamilla, X. G. Wu, and J. K. Jain, Composite fermion theory of collective excitations in fractional quantum hall effect, *Phys. Rev. Lett.* **76**, 1332 (1996).
- [69] S. M. Girvin and T. Jach, Formalism for the quantum hall effect:

- Hilbert space of analytic functions, *Phys. Rev. B* **29**, 5617 (1984).
- [70] G. Giuliani and G. Vignale, *Quantum Theory of the Electron Liquid* (Cambridge University Press, 2005).

**SUPPLEMENTAL MATERIAL FOR
“THEORY OF MAGNETOROTON BANDS IN MOIRÉ MATERIALS”**

Brillouin-zone-folded Hamiltonian

As commented in the main text, the periodic potential will couple the ground state $|\Psi_0\rangle$ to excitations with momentum equal to a reciprocal lattice vector, modifying the ground state energy E_0 . We will restrict the manifold of excitations to only contain the magnetoroton states $|\Psi_G\rangle$, as they accurately capture the long-wavelength limit of the neutral excitations, up to the magnetoroton minimum for $\nu = 1/3$ filling factor. The first-order correction to the ground state energy, that we denote $E_0^{(1)}$, vanishes in the thermodynamic limit due to continuous magnetic translation symmetry. The second order correction to the ground state energy is given by

$$E_0^{(2)} = \lambda^2 \sum_{\mathbf{G}} \frac{|\langle \Psi_{\mathbf{G}} | \bar{\rho}_{\mathbf{G}} | \Psi_0 \rangle|^2}{E_0 - E_{\mathbf{G}}} = -6\lambda^2 \frac{|\langle \bar{\rho}_{\mathbf{G}}^\dagger \bar{\rho}_{\mathbf{G}} \rangle_0|^2}{N\Delta_{\mathbf{G}}S_{\mathbf{G}}}, \quad (10)$$

where $|\Psi_{\mathbf{G}}\rangle = \bar{\rho}_{\mathbf{G}} |\Psi_0\rangle / \sqrt{NS_{\mathbf{G}}}$ is a magnetoroton excitation. In contrast, the corrections to the magnetoroton energies due to the periodic potential are of order λ , for this reason we focus our analysis on the effect of the periodic potential on the branch low-energy neutral excitations.

To obtain the Brillouin-zone-folded (BZ-folded) Hamiltonian (1), we use the normalized SMA basis (2), i.e.,

$$\langle \Psi_{\mathbf{q}'} | \Psi_{\mathbf{q}} \rangle = \frac{1}{N\sqrt{\bar{S}_{\mathbf{q}'}\bar{S}_{\mathbf{q}}}} \langle \Psi_0 | \bar{\rho}_{\mathbf{q}'}^\dagger \bar{\rho}_{\mathbf{q}} | \Psi_0 \rangle = \delta_{\mathbf{q}', \mathbf{q}}, \quad (11)$$

where $\bar{S}(\mathbf{q})$ is the projected structure factor in (4) and we have translational symmetry in the Laughlin state. Writing the Schrödinger equation in this SMA state basis, i.e., $|\Phi_{\mathbf{q}}\rangle = \sum_{\mathbf{G}} c_{\mathbf{q}+\mathbf{G}} |\Psi_{\mathbf{q}+\mathbf{G}}\rangle$ with \mathbf{q} is restricted to the Brillouin zone, and taking the inner product with $|\Psi_{\mathbf{q}+\mathbf{G}'}\rangle$ on both sides, we find

$$\sum_{\mathbf{G}} H(\mathbf{q})_{\mathbf{G}', \mathbf{G}} c_{\mathbf{q}+\mathbf{G}} = E \sum_{\mathbf{G}} c_{\mathbf{q}+\mathbf{G}} \langle \Psi_{\mathbf{q}+\mathbf{G}'} | \Psi_{\mathbf{q}+\mathbf{G}} \rangle = c_{\mathbf{q}+\mathbf{G}'}. \quad (12)$$

This leads to an eigenvalue problem for the Hamiltonian matrix and the expansion coefficients, with states within the BZ decoupled. The Hamiltonian matrix elements are $H(\mathbf{q})_{\mathbf{G}', \mathbf{G}} = \langle \Psi_{\mathbf{q}+\mathbf{G}'} | H | \Psi_{\mathbf{q}+\mathbf{G}} \rangle$. In the SMA basis, the H_0 term is diagonal:

$$H_0(\mathbf{q})_{\mathbf{G}', \mathbf{G}} = \langle \Psi_{\mathbf{q}+\mathbf{G}'} | H_0 | \Psi_{\mathbf{q}+\mathbf{G}} \rangle = \delta_{\mathbf{G}', \mathbf{G}} \langle \Psi_{\mathbf{q}+\mathbf{G}'} | H_0 | \Psi_{\mathbf{q}+\mathbf{G}} \rangle = \delta_{\mathbf{G}', \mathbf{G}} \Delta(\mathbf{q} + \mathbf{G}), \quad (13)$$

where $\Delta(\mathbf{q} + \mathbf{G})$ is the unperturbed magnetoroton dispersion, while the perturbing periodic potential V couples states related by a reciprocal lattice vector, i.e.,

$$\langle \Psi_{\mathbf{q}+\mathbf{G}'} | V | \Psi_{\mathbf{q}+\mathbf{G}} \rangle = \lambda \sum_{\tilde{\mathbf{G}}} \langle \Psi_{\mathbf{q}+\mathbf{G}'} | \bar{\rho}_{\tilde{\mathbf{G}}} | \Psi_{\mathbf{q}+\mathbf{G}} \rangle = \lambda \sum_{\tilde{\mathbf{G}}} \delta_{\mathbf{G}', \tilde{\mathbf{G}}+\mathbf{G}} \frac{1}{N\sqrt{\bar{S}_{\mathbf{q}+\mathbf{G}}\bar{S}_{\mathbf{q}+\mathbf{G}'}}} \langle \Psi_0 | \bar{\rho}_{\mathbf{q}+\mathbf{G}'}^\dagger \bar{\rho}_{\tilde{\mathbf{G}}} \bar{\rho}_{\mathbf{q}+\mathbf{G}} | \Psi_0 \rangle. \quad (14)$$

As stated in the main text, the problem thus reduces to diagonalizing the effective Hamiltonian

$$H(\mathbf{q})_{\mathbf{G}', \mathbf{G}} = \delta_{\mathbf{G}', \mathbf{G}} \Delta(\mathbf{q} + \mathbf{G}) + \lambda \sum_{\tilde{\mathbf{G}}} \delta_{\mathbf{G}', \tilde{\mathbf{G}}+\mathbf{G}} \frac{1}{N\sqrt{\bar{S}_{\mathbf{q}+\mathbf{G}}\bar{S}_{\mathbf{q}+\mathbf{G}'}}} \langle \Psi_0 | \bar{\rho}_{\mathbf{q}+\mathbf{G}'}^\dagger \bar{\rho}_{\tilde{\mathbf{G}}} \bar{\rho}_{\mathbf{q}+\mathbf{G}} | \Psi_0 \rangle. \quad (15)$$

Three-point function projected to the LLL

We use the framework proposed by Girvin and Jach [69] to project an operator that depends on z and z^* into the lowest Landau level – by replacing $z^* \mapsto 2\ell^2 \frac{\partial}{\partial z}$ – and we use complex notation $q = q_x + iq_y$. The three-point density correlation function can be split into five terms:

$$\begin{aligned}
\bar{\rho}_{q+G'}^\dagger \bar{\rho}_{\tilde{G}} \bar{\rho}_{q+G} &= \left(\sum_j e^{-i(-q-G')\ell^2 \frac{\partial}{\partial z_j}} e^{-i(-q-G')^* \frac{z_j}{2}} \right) \left(\sum_n e^{-i\tilde{G}\ell^2 \frac{\partial}{\partial z_n}} e^{-i\tilde{G}^* \frac{z_n}{2}} \right) \left(\sum_m e^{-i(q+G)\ell^2 \frac{\partial}{\partial z_m}} e^{-i(q+G)^* \frac{z_m}{2}} \right) \\
&= N e^{[-(q+G')^* \tilde{G} + \tilde{G}^* (q+G) - (q+G')^* (q+G)] \ell^2 / 2} \\
&\quad + \sum_{j \neq n \neq m} \left(e^{-i[(-q-G') \frac{\partial}{\partial z_j} + \tilde{G} \frac{\partial}{\partial z_n} + (q+G) \frac{\partial}{\partial z_m}] \ell^2} \right) \left(e^{-i[(-q-G')^* \frac{z_j}{2} + \tilde{G}^* \frac{z_n}{2} + (q+G)^* \frac{z_m}{2}] \right) \\
&\quad + \sum_{j=n \neq m} \left(e^{-i(-q-G'+\tilde{G})\ell^2 \frac{\partial}{\partial z_j}} e^{-i(q+G)\ell^2 \frac{\partial}{\partial z_m}} e^{-i(-q-G'+\tilde{G})^* \frac{z_j}{2}} e^{-i(q+G)^* \frac{z_m}{2}} \right) e^{-(q+G')^* \tilde{G} \ell^2 / 2} \\
&\quad + \sum_{j=m \neq n} \left(e^{-i(-q-G'+q+G)\ell^2 \frac{\partial}{\partial z_j}} e^{-i\tilde{G}\ell^2 \frac{\partial}{\partial z_n}} e^{-i(-q-G'+q+G)^* \frac{z_j}{2}} e^{-i\tilde{G}^* \frac{z_n}{2}} \right) e^{-(q+G')^* (q+G) \ell^2 / 2} \\
&\quad + \sum_{j \neq m=n} \left(e^{-i(-q-G')\ell^2 \frac{\partial}{\partial z_j}} e^{-i(\tilde{G}+q+G)\ell^2 \frac{\partial}{\partial z_n}} e^{-i(-q-G')^* \frac{z_j}{2}} e^{-i(\tilde{G}+q+G)^* \frac{z_n}{2}} \right) e^{\tilde{G}^* (q+G) \ell^2 / 2}. \tag{16}
\end{aligned}$$

The Laughlin-state expectation value of this operator is non-vanishing only when momentum is conserved (up to a reciprocal lattice vector), requiring \tilde{G} such that $G + \tilde{G} - G' = 0$. We can then rewrite the last three lines using full two-point functions:

$$\begin{aligned}
\bar{\rho}_{q+G'}^\dagger \bar{\rho}_{\tilde{G}} \bar{\rho}_{q+G} &= N e^{[-(q+G')^* \tilde{G} + \tilde{G}^* (q+G) - (q+G')^* (q+G)] \ell^2 / 2} \\
&\quad + \sum_{j \neq n \neq m} \left(e^{-i[(-q-G') \frac{\partial}{\partial z_j} + \tilde{G} \frac{\partial}{\partial z_n} + (q+G) \frac{\partial}{\partial z_m}] \ell^2} \right) \left(e^{-i[(-q-G')^* \frac{z_j}{2} + \tilde{G}^* \frac{z_n}{2} + (q+G)^* \frac{z_m}{2}] \right) \\
&\quad + (\overline{\rho_{-q-G} \rho_{q+G}} - N) e^{-(q+G')^* \tilde{G} \ell^2 / 2} + (\overline{\rho_{-\tilde{G}} \rho_{\tilde{G}}} - N) e^{-(q+G')^* (q+G) \ell^2 / 2} \\
&\quad + (\overline{\rho_{-q-G'} \rho_{q+G'}} - N) e^{\tilde{G}^* (q+G) \ell^2 / 2}. \tag{17}
\end{aligned}$$

Finally, in the previous expression, the term where all three indices are different ($i \neq j \neq k$) is related to the full unprojected three-point function through

$$\begin{aligned}
&\sum_{j \neq n \neq m} \left(e^{-i[(-q-G') \frac{\partial}{\partial z_j} + \tilde{G} \frac{\partial}{\partial z_n} + (q+G) \frac{\partial}{\partial z_m}] \ell^2} \right) \left(e^{-i[(-q-G')^* \frac{z_j}{2} + \tilde{G}^* \frac{z_n}{2} + (q+G)^* \frac{z_m}{2}] \right) \\
&= \left(\rho_{q+G'}^\dagger \rho_{\tilde{G}} \rho_{q+G} - N \right) - (\overline{\rho_{-q-G} \rho_{q+G}} - N) - (\overline{\rho_{-\tilde{G}} \rho_{\tilde{G}}} - N) - (\overline{\rho_{-q-G'} \rho_{q+G'}} - N). \tag{18}
\end{aligned}$$

Inserting Eq. (18) into Eq. (17) and dividing by N leads to the projected three-point function presented in the main text, and repeated here for the reader's convenience:

$$\begin{aligned}
\frac{1}{N} \langle \bar{\rho}_{q+G'}^\dagger \bar{\rho}_{\tilde{G}} \bar{\rho}_{q+G} \rangle_0 &= \frac{1}{N} \langle \rho_{q+G'}^\dagger \rho_{\tilde{G}} \rho_{q+G} \rangle_0 - \left[1 - e^{[-(q+G')^* \tilde{G} + \tilde{G}^* (q+G) - (q+G')^* (q+G)] \frac{\ell^2}{2}} \right] \\
&\quad - [S_{q+G} - 1] \left[1 - e^{-(q+G')^* \tilde{G} \frac{\ell^2}{2}} \right] - [S_{\tilde{G}} - 1] \left[1 - e^{-(q+G')^* (q+G) \frac{\ell^2}{2}} \right] - [S_{q+G'} - 1] \left[1 - e^{\tilde{G}^* (q+G) \frac{\ell^2}{2}} \right]. \tag{19}
\end{aligned}$$

The difference between products of projected and products of unprojected density operators originates from virtual transitions to higher Landau levels; the projected product vanishes in the case of a fully-filled Landau level because these are the only transitions available [70].

Derivation of the perturbative expression of the dynamical structure in the single mode approximation

In this section, we derive the perturbative expression for the optical conductivity in the SMA. The first step is to use perturbation theory for the first order correction of the wavefunctions due to the periodic potential $|\Psi_{k,m}\rangle \approx |\Psi_{k,m}^{(0)}\rangle + |\Psi_{k,m}^{(1)}\rangle$ where

$$|\Psi_{k,m}^{(1)}\rangle = \sum_{G,n} \lambda_G \frac{\langle \Psi_{k+G,n}^{(0)} | \bar{\rho}_G | \Psi_{k,m}^{(0)} \rangle}{E_{k,m}^{(0)} - E_{k+G,n}^{(0)}} |\Psi_{k+G,n}^{(0)}\rangle, \tag{20}$$

to calculate the dynamical structure factor

$$S(\mathbf{q}, \epsilon) = \frac{1}{N} \sum_{m>0} |\langle \Psi_m | \bar{\rho}_{\mathbf{q}} | \Psi_0 \rangle|^2 \delta[\epsilon - (E_m - E_0)], \quad (21)$$

where m labels the excited states ($m = 0$ labels the ground state). Keeping only leading order terms in λ and noting that the unperturbed states matrix elements $\langle \Psi_{\mathbf{q},m}^{(0)} | \bar{\rho}_{\mathbf{q}} | \Psi_0^{(0)} \rangle$ scale as $|\mathbf{q}|^2$ in the long wavelength limit, so they will not contribute to the optical conductivity

$$\text{Re } \sigma(\omega) = \frac{\pi e^2 N}{A} \lim_{q \rightarrow 0} [\omega S(\mathbf{q}, \hbar\omega) / q^2], \quad (22)$$

the only leading order term that contributes to the dynamical structure factor is

$$\langle \Psi_{\mathbf{k},m}^{(0)} | \bar{\rho}_{\mathbf{q}} | \Psi_0^{(1)} \rangle = \sum_{\mathbf{G},n} \lambda_{\mathbf{G}} \frac{\langle \Psi_{\mathbf{G},n}^{(0)} | \bar{\rho}_{\mathbf{G}} | \Psi_0^{(0)} \rangle}{E_0^{(0)} - E_{\mathbf{G},n}^{(0)}} \langle \Psi_{\mathbf{q}+\mathbf{G},m}^{(0)} | \bar{\rho}_{\mathbf{q}} | \Psi_{\mathbf{G},n}^{(0)} \rangle \delta_{\mathbf{k},\mathbf{q}+\mathbf{G}} \quad (23)$$

Substituting Eq. (23) in Eq. (21), we get

$$S(\mathbf{q}, \epsilon) = \frac{1}{N} \sum_{\mathbf{G},m} \left| \sum_n \lambda_{\mathbf{G}} \frac{\langle \Psi_{\mathbf{q}+\mathbf{G}}^{(0)} | \bar{\rho}_{\mathbf{q}} | \Psi_{\mathbf{G},n}^{(0)} \rangle \langle \Psi_{\mathbf{G},n}^{(0)} | \bar{\rho}_{\mathbf{G}} | \Psi_0^{(0)} \rangle}{E_0^{(0)} - E_{\mathbf{G},n}^{(0)}} \right|^2 \delta[\epsilon - (E_{\mathbf{q}+\mathbf{G},m}^{(0)} - E_0^{(0)})]. \quad (24)$$

where we have not included the excitation energy shifts which are formally of higher order in $\lambda_{\mathbf{G}}$. Next, we employ the SMA $|\Psi_{\mathbf{q}}\rangle = \frac{1}{\sqrt{\bar{S}_{\mathbf{q}} N}} \bar{\rho}_{\mathbf{q}} |\Psi_0\rangle$ so that

$$S(\mathbf{q}, \epsilon) = \frac{1}{N} \sum_{\mathbf{G}} \left| \lambda_{\mathbf{G}} \frac{\langle \Psi_{\mathbf{q}+\mathbf{G}} | \bar{\rho}_{\mathbf{q}} | \Psi_{\mathbf{G}} \rangle \langle \Psi_{\mathbf{G}} | \bar{\rho}_{\mathbf{G}} | \Psi_0^{(0)} \rangle}{\Delta_{\mathbf{G}}} \right|^2 \delta(\epsilon - \Delta_{\mathbf{q}+\mathbf{G}}), \quad (25)$$

and noting that the second expectation value in the numerator $\langle \Psi_{\mathbf{G}} | \bar{\rho}_{\mathbf{G}} | \Psi_0^{(0)} \rangle = \sqrt{N \bar{S}_{\mathbf{G}}}$, Eq. (25) becomes

$$S(\mathbf{q}, \epsilon) = \sum_{\mathbf{G}} \left| \lambda_{\mathbf{G}} \frac{\langle \Psi_0^{(0)} | \bar{\rho}_{\mathbf{q}+\mathbf{G}} \bar{\rho}_{\mathbf{q}} \bar{\rho}_{\mathbf{G}} | \Psi_0^{(0)} \rangle}{N \sqrt{\bar{S}_{\mathbf{q}+\mathbf{G}}} \Delta_{\mathbf{G}}} \right|^2 \delta(\epsilon - \Delta_{\mathbf{q}+\mathbf{G}}). \quad (26)$$

We now examine the small \mathbf{q} limit of the three point function $\langle \bar{\rho}_{\mathbf{q}+\mathbf{G}}^\dagger \bar{\rho}_{\mathbf{q}} \bar{\rho}_{\mathbf{G}} \rangle_0$. Since there are no dipole allowed transitions within the lowest Landau level $\bar{\rho}_{\mathbf{q}} |\Psi_0\rangle = 0$ to first order in $|\mathbf{q}|$. Therefore, we can replace $\bar{\rho}_{\mathbf{q}} \bar{\rho}_{\mathbf{G}}$ by the commutator $[\bar{\rho}_{\mathbf{q}}, \bar{\rho}_{\mathbf{G}}]$ (since the second term will vanish by the argument above in the long wavelength limit). Using the GMP algebra,

$$\begin{aligned} \langle \bar{\rho}_{\mathbf{q}+\mathbf{G}}^\dagger \bar{\rho}_{\mathbf{q}} \bar{\rho}_{\mathbf{G}} \rangle_0 &= \langle \bar{\rho}_{\mathbf{q}+\mathbf{G}}^\dagger [\bar{\rho}_{\mathbf{q}}, \bar{\rho}_{\mathbf{G}}] \rangle_0 = (e^{q^* G \ell^2 / 2} - e^{G^* q \ell^2 / 2}) \langle \bar{\rho}_{\mathbf{q}+\mathbf{G}}^\dagger \bar{\rho}_{\mathbf{q}+\mathbf{G}} \rangle_0 \\ &= N (e^{q^* G \ell^2 / 2} - e^{G^* q \ell^2 / 2}) \bar{S}_{\mathbf{q}+\mathbf{G}} \end{aligned} \quad (27)$$

Expanding the exponentials to first order in q :

$$(e^{q^* G \ell^2 / 2} - e^{G^* q \ell^2 / 2}) = 1 + \frac{q^* G \ell^2}{2} - 1 - \frac{G^* q \ell^2}{2} + O(q^2) = i \ell^2 (\mathbf{q} \times \mathbf{G})_{\hat{z}} + O(q^2) \quad (28)$$

so to leading order in q

$$\langle \bar{\rho}_{\mathbf{q}+\mathbf{G}}^\dagger \bar{\rho}_{\mathbf{q}} \bar{\rho}_{\mathbf{G}} \rangle_0 / N = i \ell^2 (\mathbf{q} \times \mathbf{G})_{\hat{z}} \bar{S}_{\mathbf{q}+\mathbf{G}} \quad (29)$$

Next, we compare this expression to the MC simulations result. In Fig. 4 we plot the left-hand-side of Eq. (29) obtained from the MC simulations and the long-wavelength limit (right-hand-side of Eq. (29) for a representative $\mathbf{G} = |\mathbf{G}|(-1, 0)$. Fig. (4) shows the two expressions agree for small \mathbf{q} and provides a range of validity for this long wavelength limit.

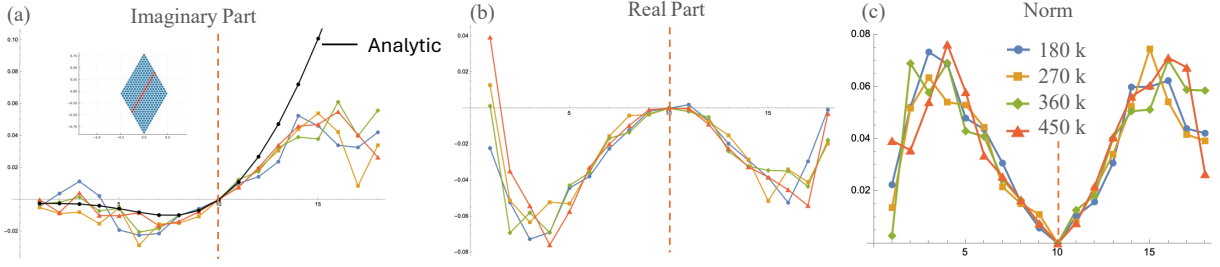


FIG. 4. Comparison the the numerical and analytical expressions of the long wavelength limit of the three point function's (29) imaginary part (a), real part (b), and norm (c), for a line cut across the BZ mesh indicated in the inset of (a). The dashed line corresponds to $q = 0$. The different lines are different number of MC samples shown in (c).

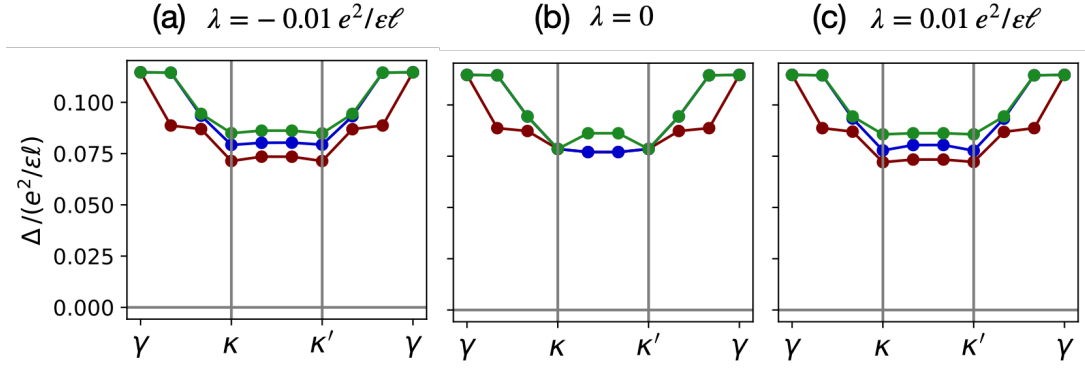


FIG. 5. Three lowest magnetoroton bands for three values of the potential strength and for one flux quantum per unit cell. The path in the Brillouin zone is the same as the one indicated in Fig. 2(a) in the main text. The κ/κ' points where the magnetoroton softening occurs are indicated by vertical lines.

Additional magnetoroton band structure results

In Fig. 5 we show the three lowest magnetoroton bands, obtained from diagonalizing Eq. (5) in the main text, for the case of one flux quantum per unit cell. In the absence of the potential, $\lambda = 0$, there is a three-fold degeneracy at κ/κ' , and a two-fold degeneracy across the line between κ and κ' , as expected. When the potential is turned-on, the three states at κ/κ' split, as do the two states on the edges of the Brillouin zone. For $\lambda = 0$ the magnetoroton minimum is located approximately at the m -point, once the hexagonal potential is introduced the magnetoroton minimum shifts to κ/κ' , due to stronger level repulsion between the three coupled states. We observe that for $|\lambda| > 0.01e^2/\epsilon\ell$ the third magnetoroton band already merges into the continuum of particle-hole excitations.